Analysis of deposit accumulated on electrodes of the compact muon solenoid (CMS) gas detectors, in the course of CSC longevity tests using 40% Ar, 50% CO_2 and 10%CF_4 gas mixture

Aleksandra Radulovic[1]*, Dubravka Milovanovic[1], Nebojsa Begovic[1], Milica Marceta Kaninski[1], Janez Kovac[2], Jernej Ekar[2], Gennady Gavrilov[3], Katerina Kuznetsova[3,4], Andrey Korytov[4], Guenakh Mitselmakher[4], Armando Lanaro[5], Petar Adzic[6], Predrag Milenovic[6]

[1]Institute of General and Physical Chemistry, Belgrade, Serbia
[2]Jozef Stefan Institute
[3]NRC Kurchatov Institute PNPI, St. Petersburg, RU
[4]University of Florida, USA
[5]University of Wisconsin Madison, USA
[6]Faculty of Physics, University of Belgrade, Belgrade, Serbia

Aleksandra
Dubravka
Nebojsa

Abstract

The application timespan and sensitivity of the muon particle detectors heavily depend on the longevity/efficiency/quality of the adjoining components. After prolonged period of operation, the used gas mixtures based on CF_4, CO_2 and argon, may significantly alter the electrodes' active surface, disrupting the morphological features and possibly even chemical composition, in form of deposits or breaches, and therefore causing their aging and replacement.

Synergetic effect of radiation and plasma chemical reaction leads to formation of deposit on the electrode surfaces thus causing degradation of operating characteristicsof gaseous detectors and limitingtheir long-termuse in particle physics experiments.

Various surface complementary analytical techniques were employed for detailed characterization of deposit accumulated on the surface of electrodes subjected to a long term exposure of β-source ^{90}Sr in the gas mixture of 40% Ar, 50% CO_2 and 10%CF_4, in the course of CSC longevity tests. Surface morphology of the electrodes was studied using microscopic techniques (OM, AFM and SEM), while chemical composition was analyzed by energy dispersive x-ray spectroscopic technique (EDS). Electronic/oxidation states of detected elements and elemental depth profiling were obtained using photoelectron (XPS) while additional information about the depth distribution and the types of species on the surface is investigated by TOF-SIMS, Chemical bonding between atoms and functional groups were studied by vibrational (FTIR and Raman) spectroscopic techniques. Insights into crystal and amorphous structures of phases constituting deposit were obtained by diffraction technique (XRD). Formation mechanisms of phases detected as deposit on the cathode surface were proposed.

1. Introduction

Literature review ….

-why do we examine aging effect in gaseous detectors

-cathode aging: what are the deposits on the cathode surface and how they affect gas chamber function (Malter effect) - formation of oxides or polymers on the surface of the cathode - originating from gas mixture components (ion and radicals formed in plasma avalanche or desorption of structural materials - Si is the product of desorption of structural materials….

-anode wire aging – Au layer cracking and formation of tungsten oxides (gas gain reduction), carbon deposition problem…

Aim of this work: detailed analysis of the microstructure of the deposit formed on electrode surfaces using numerous complementary techniques will enable better understanding of the deposition mechanism, which can further help in evaluating optimal working conditions of proportional gas chambers (selecting optimal gas mixture, construction materials of the detector such as electrode material, fiberglass used, circulation pump, gas system connections…)

Deposit accumulated on the electrodes was analyzed using various characterization techniques. Surface morphology of the electrodes was studied using microscopic techniques (OM, AFM and SEM), while chemical composition was analyzed by energy dispersive x-ray spectroscopic technique (EDS). Electronic/oxidation states of detected elements and elemental depth profiling were obtained using photoelectron (XPS) while additional information about the depth distribution and the types of species on the surface is investigated by TOF-SIMS, Chemical bonding between atoms and functional groups were studied by vibrational (FTIR and Raman) spectroscopic techniques. Insights into crystal and amorphous structures of phases constituting deposit were obtained by diffraction technique (XRD).

2. Experimental

2.1. Longevity tests

Longevity studies were performed at the Petersburg Nuclear Physics Institute (PNPI) with laboratory prototypes of multiwire cathode strip chambers (CSCs) of the CMS experiment.

2.1.1. Irradiation conditions in longevity test ***[from Gennady`s publications]***

An emitter consisting of three individual ^{90}Sr β sources (E_{β}^{max} = 2.28 MeV) in a lead container was used for aging of CSC unit prototypes. Most electrons of the spectrum of ^{90}Sr have energy which exceeds the threshold level of formation of radiation defects in metals, ~0.5 MeV, and is comparable to the energy of the electrons of background in the CMS muon tracker, ~1 MeV. The electron flux density in the process of irradiation of the CSC prototype was $F \approx 4.36 \times 106$ s^{-1} cm^{-2} and has provided an ionization current of 17 μA in the detector. The aim of this test was obtaining the upper estimate of the radiation resistance of the proportional chamber with the working gas mixture 40%Ar + 50%CO_2 + 10%CF_4. The accumulated charge in the CSC prototype was 1.36 C cm^{-1} within the time of the test of 2.1×10^6 s, which corresponds to almost 100 years of work of full-scale CSCs at the HL-LHC. The CSC prototype has conserved its working characteristics and does not exhibit any manifestations of the Malter effect. Detail description of experimental setup (irradiation conditions and scheme of the CSC prototype) are given in Buzoveria et al. **(*ref.* *Physics of Atomic Nuclei, 2019, Vol. 82, No. 9, pp. 1252–1262)***.

2.1.2. Specimens for analytical study

The cathode panels were made of polycarbonate plates with a honeycomb hexagonal structure with a thickness of 1.6 cm. The plates were fixed between the sheets of foil-coated glass-reinforced FR4 plastic with a thickness of 0.15 cm. The thickness of copper foil is 35 μm. After aging test, the specimen of foil-coated glass-reinforced plastic in the shape of disks with a diameter of 2.3 cm were sawn up from the cathode panel for investigation. The anode were gold-plated tungsten wires 50 μm in diameter (Saratov Wireplant, Russia) with specified gold plating of 5.2% by weight. The anode wires were plated using gold in the liquid phase. This technology of gold plating provides both the best surface quality and gold adhesion to the tungsten. The thickness of the gold layer evaluated using the Nuclear Reaction Analysis method ***[from Gennady`s publication]*** was about 1 mm [***ref.*** *G. Gavrilov, A. Krivchitch, V. Lebedev, Nuclear Instruments and Methods in Physics Research Section A 515 (2003) 108,* ***ref.*** *G.E. Gavrilov et al. / Nuclear Instruments and Methods in Physics Research A 694 (2012) 167–172*]. Wires were then soldered to the anode bars with spacing of about 3.2 mm.

2.2 Characterization techniques

2.2.1. Optical Microscopy

For preliminary examination of electrode surface *Motic AE200MET* metallurgy reflection optical microscope was employed.

2.2.2. Atomic Force Microscopy

Surface roughness was studied using atomic force microscopy (AFM) with AutoProbe CP-Research SPM (TM Microscopes-Bruker). The measurements were performed by implementing non-contact AFM imaging and 90 µm large area scanner. Probes Bruker Phosphorous (n) doped silicon Tap300, model MPP-11123-10 with Al reflective coating and symmetric tip were used. Driving frequency of the cantilever was about 310 kHz. AFM images were taken and later analyzed using the software Image Processing and Data Analysis Version 2.1.15 and SPMLab Analysis, DI SPMLab NT Ver. 6.0.2. AFM measurements were performed only on cathode sample due to small diameter of the anode wire.

2.2.3. Scanning Electron Microscopy and Energy Dispersive X-ray Spectroscopy

Scanning electron microscopy (SEM) with energy dispersive spectrometry (EDS) was employed for morphological and micro-elemental analysis. Measurements were performed on *JEOL JSM 6610 LV (Japan)* scanning electron microscope in conjunction with the EDS detector model *X-Max Large Area Analytical Silicon Drift* connected with *INCAEnergy 350 Microanalysis* (detection of elements Z≥5, detection limit: ~ 0.1mas.%, resolution 126 eV). The element used for optimization was nickel. Before SEM measurements were conducted, samples had been positioned on adhesive tape fixed to specimen tabs. Micrographs were recorded with different magnifications, while EDS micro-chemical analyses were done in selected points and areas. In order to determine the distribution of the deposited elements, EDS elemental mapping was performed.

2.2.4. X-ray photoelectron spectroscopy (XPS)

XPS analyses were performed on the PHI-TFA XPS spectrometer equipped with the Al-monochromatic source. The analyzed area was 0.4 mm in diameter. The pass energy during the recording of the high-energy resolution spectra was 29 eV. Two analyses were performed on every sample and reproducible spectra were obtained. The low energy electron flood gun was used during measurements to avoid possible charging. In addition, C 1s peak representing C-C/C-H bonds was shifted to 284.8 eV for referencing the binding energy scale. Multipak ver. 9.9 software was used for XPS spectra deconvolution. Uncertainty of binding energies of measured peaks is ±0.3 eV.

2.2.5. Time of light - secondary ion mass spectroscopy (ToF-SIMS)

ToF-SIMS method can be used to get additional information about the depth distribution and the types of species on the surface (especially organics, if present).ToF SIMS analyses was performed only on cathode, due to small diameter of the anode. Negative ions emitted from surface were analysed. Sputtering (etching rate) was about 0.1 nm/s. Area of 100 x 100 microns was analysed and analyses depth in SIMS was 1-2 nm. Quantitative analyses (in %) is not possible with SIMS technique. The analyses were done using TOF SIMS 5 instrument, producer ION TOF, Germany. Excitation of ions by Bi3 ion beam, 30 keV energy. Depth profiling by sputtering by Cs, 1 keV ion beam energy.

2.2.6. X-ray Diffraction

The X-ray diffraction analysis was conducted on *Rigaku Smartlab* automated multipurpose X-ray Diffractometer in θ-θ geometry (the sample in horizontal position) in para-focusing Bragg-Brentano geometry using D/teX Ultra 250 strip detector in 1D XRF suppression mode with $CuK_{\alpha 1,2}$ radiation source (U = 40 kV and I = 30 mA). The XRD pattern was collected in 3-120°2θ, with step of 0.01°, and data collection speed of 2°/min. The crystal phases were identified in dedicated *Rigaku* PDXL 2.0 software (with implemented ICCD PDF-2 2016 database). Analyzed area was ~15x15mm (depending of θ-θ geometry during data sampling), with penetration depth < 1mm (depending of the investigated material). Detection limit of the instrument is 1%. XRD measurements were performed only on cathode sample due to small diameter of the anode wire.

2.2.7. Fourier-Transform Infrared Spectroscopy

Infrared spectra were recorded on *Thermo Scientific Nicolet 6700* Fourier transform infrared (FTIR) spectrometer, using the Smart Orbit unit diamond attenuator of total reflection (ATR). Spectra were recorded in wavenumber interval from 4000 to 500 cm^{-1}, with resolution of 4 cm^{-1}.

2.2.8. Raman Spectroscopy

Raman spectra were recorded using *XploRA ONE™ (Horiba Jobin Yvon, Paris, France)* Raman microscope equipped with Nd/YAG laser with excitation wavelength (λexc) 532 nm. The powdered sample was placed on an X-Y motorized sample stage. The laser beam was focused on the sample using an objective magnification ×???. The scattered light was analyzed by the spectrograph with a grating having 1200 lines/mm, with resolution of 3 cm^{-1}. Spectra were recorded in wavenumber interval from 4000 to 500 cm^{-1}.

3. Results

3.1.Analysis of cathode sample

3.1.1. Analysis of morphology

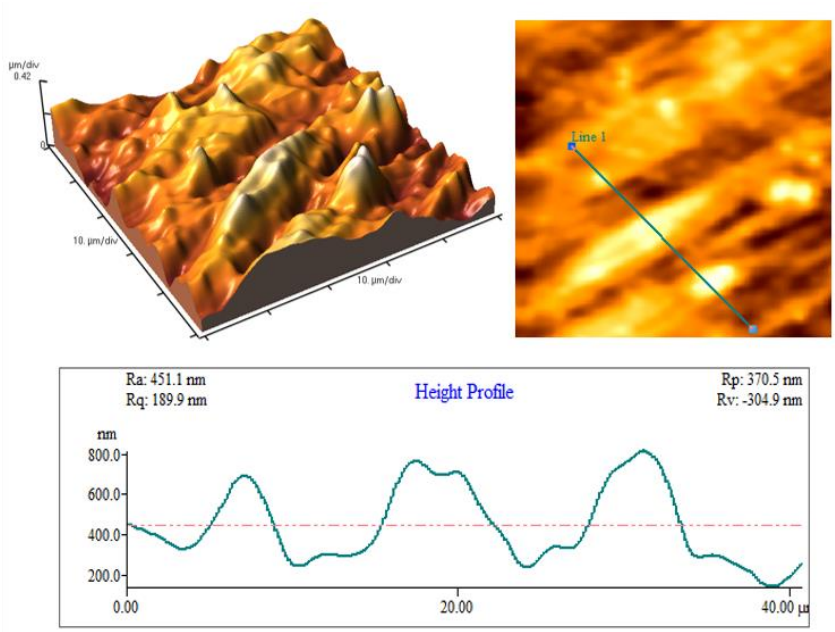

Figure 1. *AFM analysis of the cathode surface: (a) 3D AFM image of the cathode surface area 50 x 50 µm, (b) 2D AFM image with scanning line 40 µm in length along specific direction on cone-like structures and (c) surface profile measured along the scanning line with calculated roughness parameters: Average roughness Ra, RMS Roughness Rq, Maximum profile peak height Rp and Maximum profile valley depth Rv*

Morphological and roughness analysis of cathode surface by atomic force microscopy is given in Figure 1. Three-dimensional AFM image of scanned 50 x 50 µm field shows formation of complex micro-relief as a result of synergetic effect of irradiation impact and plasma chemical reactions on the copper foil surface. It can be observed that quasi-periodic pattern in the shape of alternating crests and dips, originating from fibrous structure of FR4 material, is to some degree maintained. Numerous cone-shaped micropeaks with a height of ~0.4 µm formed at the crests of the fibers can be observed. In order to estimate the roughness of the cathode surface, profile along specific direction 40 µm in length on cone-like structures was analyzed. On specified length, three crests with formed micropeaks can be distinguished. The width of crests is ~7-10 µm, with height ~ 0.8 µm, while the depth of interstructural dips is ~ 0.2 µm. Calculated (estimated) average value of roughness along scanned line is 0.451 µm with maximum profile peak height 0.370 µm, while maximum profile valley depth is 0.305 µm.

Figure 2 (a-d) shows morphological (SEM) and micro-elemental (EDS) analysis of cathode surface. An overview micrograph of the selected area (~3.5x3.5mm, magnification x36) (Figure 2(a)) showed light and dark zones on the cathode surface. Micro-elemental analysis

(Fig. 2 (b)) revealed light areas are characterized by higher amount of fluorine (wt % (F) = 8.81-9.0) and lower amount of carbon (wt % (C) = 10.2-10.65) compared to dark areas (wt % (F) = 4.44-5.44) and (wt % (C) = 12.07-12.61). At higher magnifications (Fig. 2 (c, d)), characteristic morphology (single structural elements) intrinsic to radiation erosion effect and deposited species formed in plasma chemical reaction in the form of blisters and craters can be observed. Micro-elemental analysis performed in several areas and points showed high concentration of fluorine and oxygen in blisters (wt % (F) = 18.42-17.20, wt % (O) = 16.91-15.99), followed by significant concentration of silicon (wt % (Si) = 3.04-2.71) (Figure 2 (d), Spectrum 5 and 6). As amount of fluorine decreases (from 18.42 to 3.98 wt % (F)), lowering of silicon content (from 3.04 to 0.14 wt % (Si)) can be detected. This trend can indicate formation of silicon-oxide-fluoride compounds in the course of deposition process.

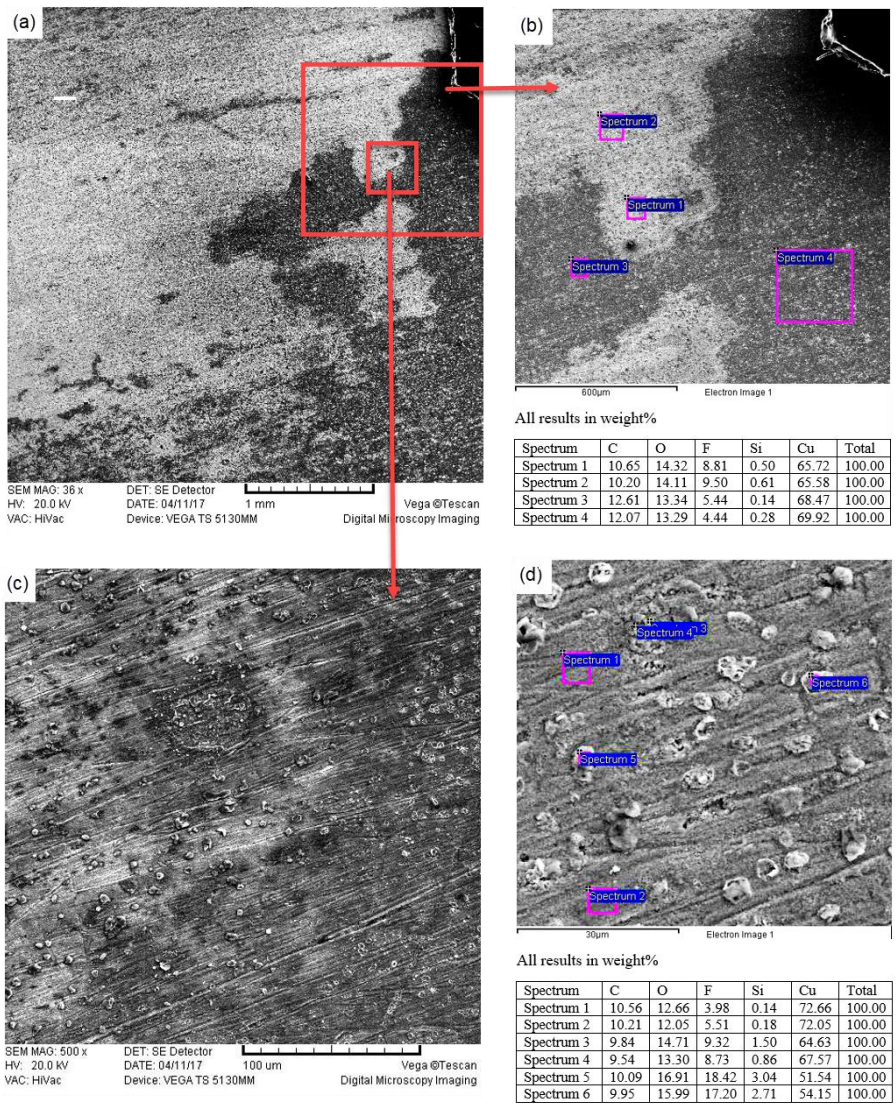

All results in weight%

Spectrum	C	O	F	Si	Cu	Total
Spectrum 1	10.65	14.32	8.81	0.50	65.72	100.00
Spectrum 2	10.20	14.11	9.50	0.61	65.58	100.00
Spectrum 3	12.61	13.34	5.44	0.14	68.47	100.00
Spectrum 4	12.07	13.29	4.44	0.28	69.92	100.00

All results in weight%

Spectrum	C	O	F	Si	Cu	Total
Spectrum 1	10.56	12.66	3.98	0.14	72.66	100.00
Spectrum 2	10.21	12.05	5.51	0.18	72.05	100.00
Spectrum 3	9.84	14.71	9.32	1.50	64.63	100.00
Spectrum 4	9.54	13.30	8.73	0.86	67.57	100.00
Spectrum 5	10.09	16.91	18.42	3.04	51.54	100.00
Spectrum 6	9.95	15.99	17.20	2.71	54.15	100.00

Figure 2. *SEM and EDS analysis of the cathode surface: (a) overview micrograph of the cathode surface (area ~ 3.5x3.5mm, magnification x36), (b) EDS results in selected areas, (c) micrograph of selected area (~250µm, magnification x500) and (d) EDS results in selected areas and points.*

Should we note that EDS analysis of elemental composition on the microstructural scale is semiquantitative analysis and is considered only indicative?

In order to further analyze distribution of discussed elements, EDS mapping of the cathode surface was performed. The EDS mapping shows spatial distribution of individual elements within an inspection field, specified by distinctive colors, while the bright spots in the EDS mapping correspond to a high concentration of the mapped element. Cumulative elemental map and EDS spectrum are presented in Figure 3 (a, b), while mapping results for individual elements are given in Figures 3 (c-g). The colors representing the Cu, O, F, Si and C elements are blue, green, purple, red and yellow, respectively. Inspection field was ~ 75x55 µm. Individual elemental maps of O, F and Si are characterized with matching distribution, showing the highest concentration in the same zones, whereas distribution of C did not follow this trend.

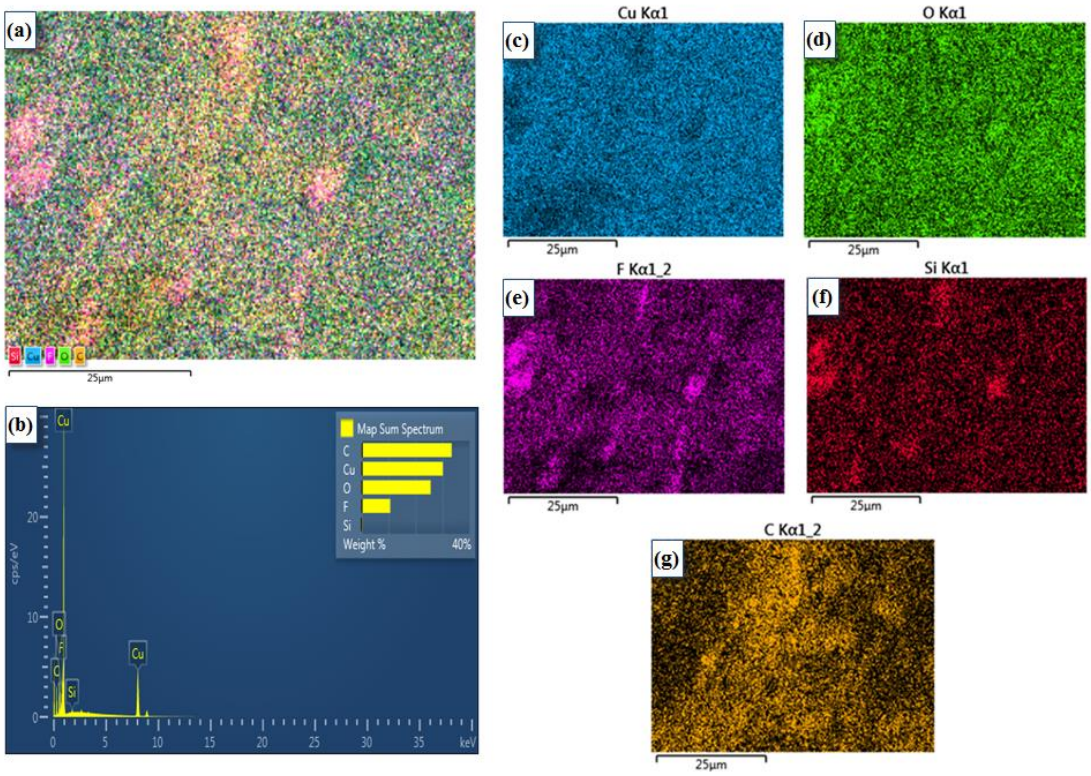

Figure 3. *SEM-EDS elemental map analysis of selected area of the cathode surface: (a) cumulative elemental mapping analysis, (b) EDS spectrum, (c-g) elemental mapping results as a function of individual elements Cu, O, F, Si and C.*

To further investigate potential formation of chemical bonds between detected elements, X-ray photoelectron spectroscopy (XPS) and time of light secondary ion mass spectroscopy (ToF-SIMS) were employed.

XPS analyses were performed in order to get insight in surface chemistry/composition of cathode and anode samples subjected to a long term exposure of β-source ^{90}Sr in the gas mixture of 40% Ar, 50% $CO_2$and 10%CF_4, in the course of CSC longevity tests. XPS spectra Cu $2p_{3/2}$ and C 1s from surface of new (virgin) and exposed cathode are presented in Figure 4. XPS depth profile recorded on thenew and exposed cathodes are shown in Figures 5a and 5b. Profiling was done up to about 20 nm depth. The new cathode shows the presence of C and O in the top surface layer, which is probably related with surface contamination and oxidation. Cu $2p_{3/2}$ spectrum shows a peak at 934.3 eV and plasmon structures at 941 and 944 eV, both characteristic for Cu^{2+} oxidation state of Cu, probably related with a thin CuO surface oxide layer, Figure 4a. In addition a peak at 932.7 eV is present and it is related to Cu-metallic matrix, which is present beneath the CuO layer as can be seen in the XPS depth profile bellow, Figure 5a. Carbon C 1s spectra shows peaks characteristic for carbon contamination (C-C/C-H bonds at 284.8 eV, C-O/C-OH bonds at 286 eV and O=C-O bonds at 289 eV), Figure 4b.

After the exposure the Cu 2p spectrum shows again the Cu(2+) oxidation state, but the metallic Cu is not present in the surface spectrum of Cu 2p as it was in the spectrum from the new cathode, Figure 4c. Carbon C 1s spectrum from exposed cathode shows strong dominating peak at 284.8 eV related with C-C/C-H bonds, figure 4d. This is probably related with a graphitic-like deposit on the cathode surface after exposure as it is evidenced by XPS depth profile bellow, Figure 5b.

Figure 5b shows an XPS depth profile up to 18 nm in depth of the exposed cathode. It differs a lot from unexposed cathode. Relatively high carbon presence on the surface, ~ 87 at.%, is probably either due to surface contamination or the residues during the interaction of gas molecules with the surface of cathode during exposure. However, the carbon atomic concentration is not decreased even at the 20 nm depth. This implies that the presence of carbon below surface can be attributed to the carbon deposit, in graphite form. Additionally, the Cu and O were identified at the cathode surface, ~ 8 at.% and 5 at.%, respectively, with the spectrum of copper corresponding to Cu^{2+} oxidation state, e.g. CuO compound. Since XPS is semi-quantitative analysis, the compound identification had to be validated/confirmed by other techniques. The overall conclusion is the C agglomerates are present at the cathode surface and so the cathode base material Cu, is emerging through these agglomerates. It is interesting to note that also traces of F (not shown in profile) and about 3 at.% of Si were detected in the subsurface region of the exposed cathode. The origin of F is probably interaction of CF4 with cathode, but the origin of Si is not clear yet. It may origin from the glass fibres incorporated into FR4 substrate.

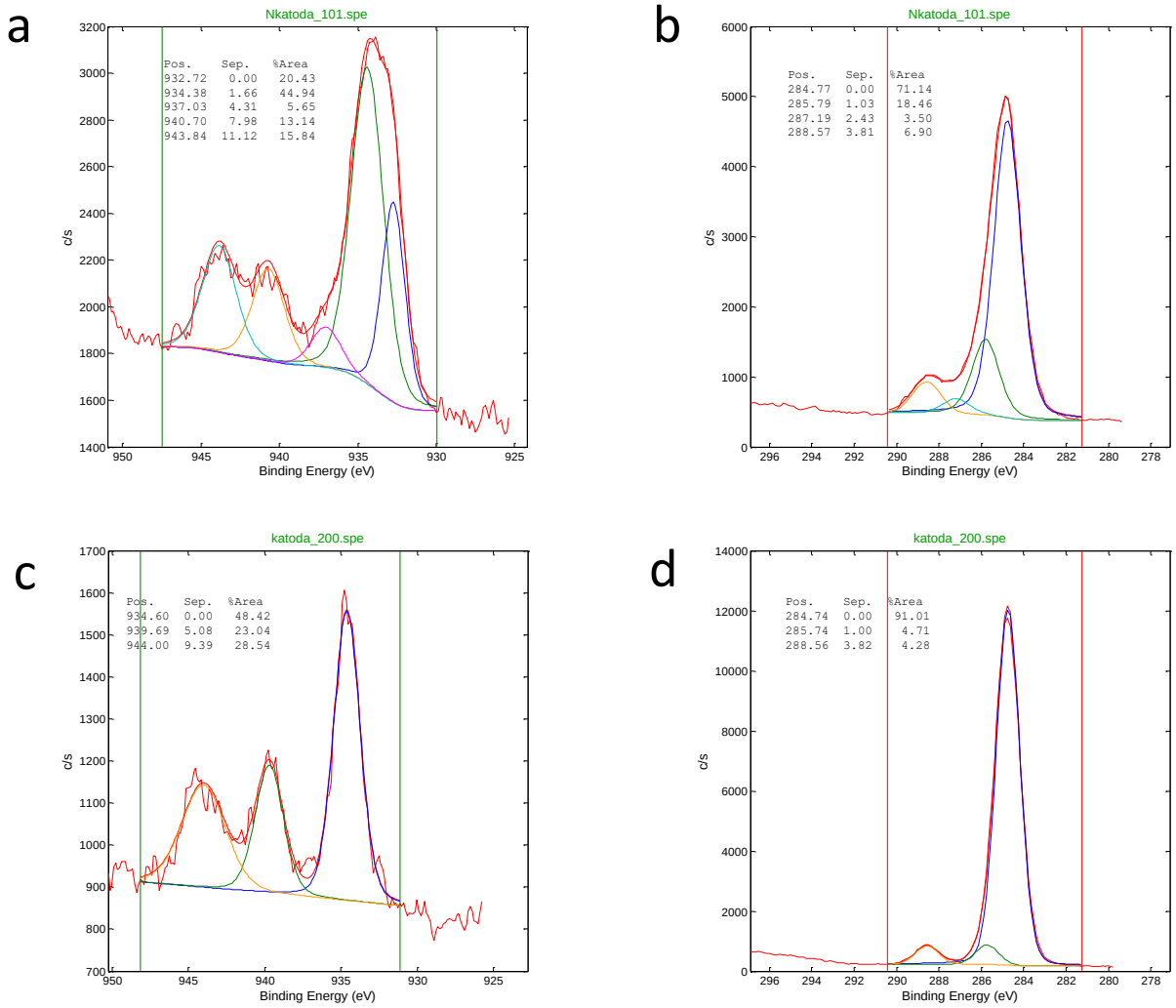

Figure 4. XPS spectra Cu $2p_{3/2}$ and C 1s from surface of (a, b) new and (c, d) exposed cathode.

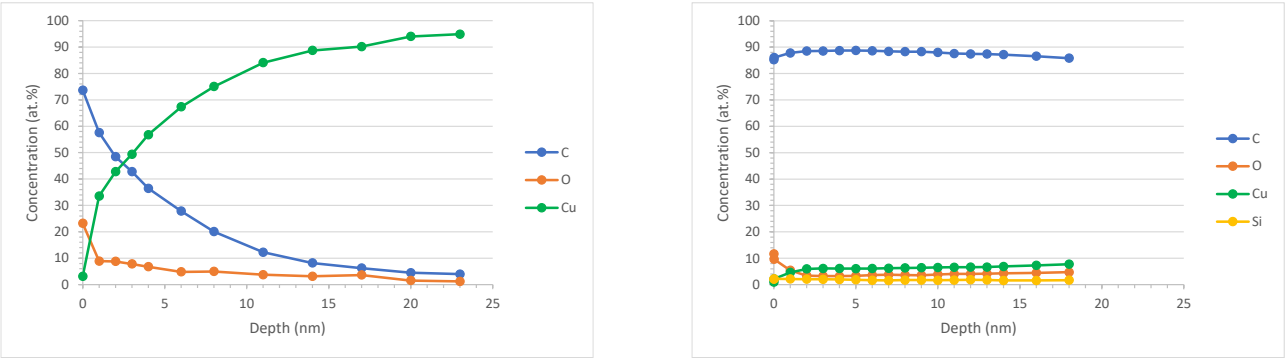

Figure 5. XPS depth profiles recorded on (a) the non-exposed cathode and (b) cathode subjected to a long term exposure of β-source ^{90}Sr in the gas mixture of 40% Ar, 50% CO_2 and 10%CF_4, in the course of CSC longevity tests.

SIMS depth profiles of selected signals obtained on CERN cathode versus depth are presented in Figure 6. The results show the cathode contains Cu, probably covered with Cu-oxide. Cathode surface also contains elements C, Cl, S, C-N, possibly due to contamination or interaction during operation. Beneath the surface region is a region rich with F (also detected by XPS analysis?), probably interacting with Cu and Cu-oxide. This region is about 300 nm thick. Beneath the Cu-oxide, also B-oxide signal appeared (?)

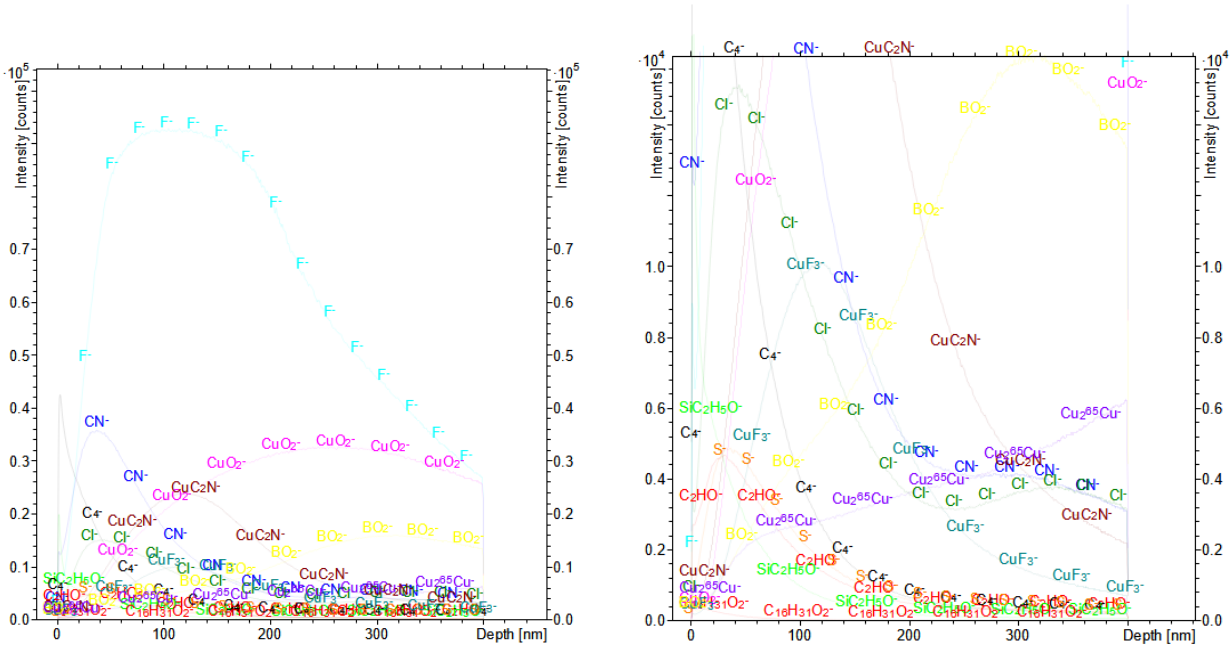

a) b)

Figure 6. SIMS depth profiles of selected signals obtained on CERN cathode versus depth (a) and depth, scale adopted for small signals (b).

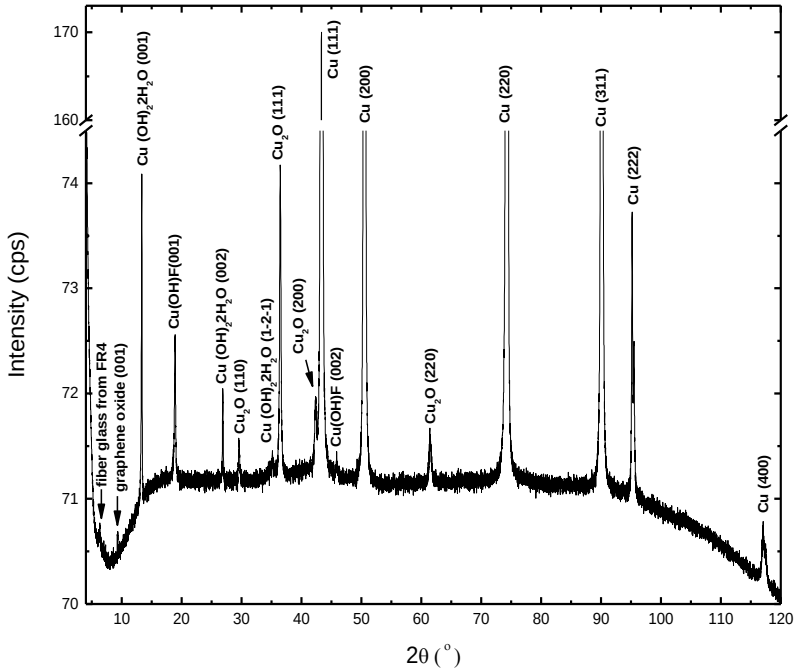

Figure 7. *XRD pattern of the cathode surface*

XRD pattern of the cathode surface is shown in Fig. 7. Beside high intensity diffraction peaks characteristic for Cu crystal phase (ICDD PDF card 00-004-0836) originating from copper foil, diffraction peaks of lower intensity corresponding to crystal phases: cuprite Cu_2O (ICDD PDF card 00-005-0667), copper hydroxide hydrate $Cu(OH)_2H_2O$ (ICDD PDF card 00-042-0746) and copper hydroxide fluoride Cu(OH)F (ICDD PDF card 01-074-3547) can be detected. Diffraction peaks at 29.5°, 36.4°, 42.4° and 61.5° 2θ originate from cubic Cu_2O phase and correspond to diffraction from (110), (111), (200) and (220) crystal planes. Peaks at 13.4°, 26.8° and 35.1° 2θ can be attributed to diffraction from (001), (002) and (1-2-1) crystal planes of triclinic $Cu(OH)_2H_2O$ phase, while peaks at 18.9° and 45.8° 2θ correspond to diffraction from (001) and (002) crystal planes of cubic Cu(OH)F phase. Two low intensity diffraction peaks at angles below 10° 2θ can also be detected in XRD pattern: diffraction peak at ~9.30 2θ can be attributed to diffraction from crystal plane (100) of graphene oxide, while peak at ~6.30° 2θ can be assigned to fiber glass originating from FR4 laminate.

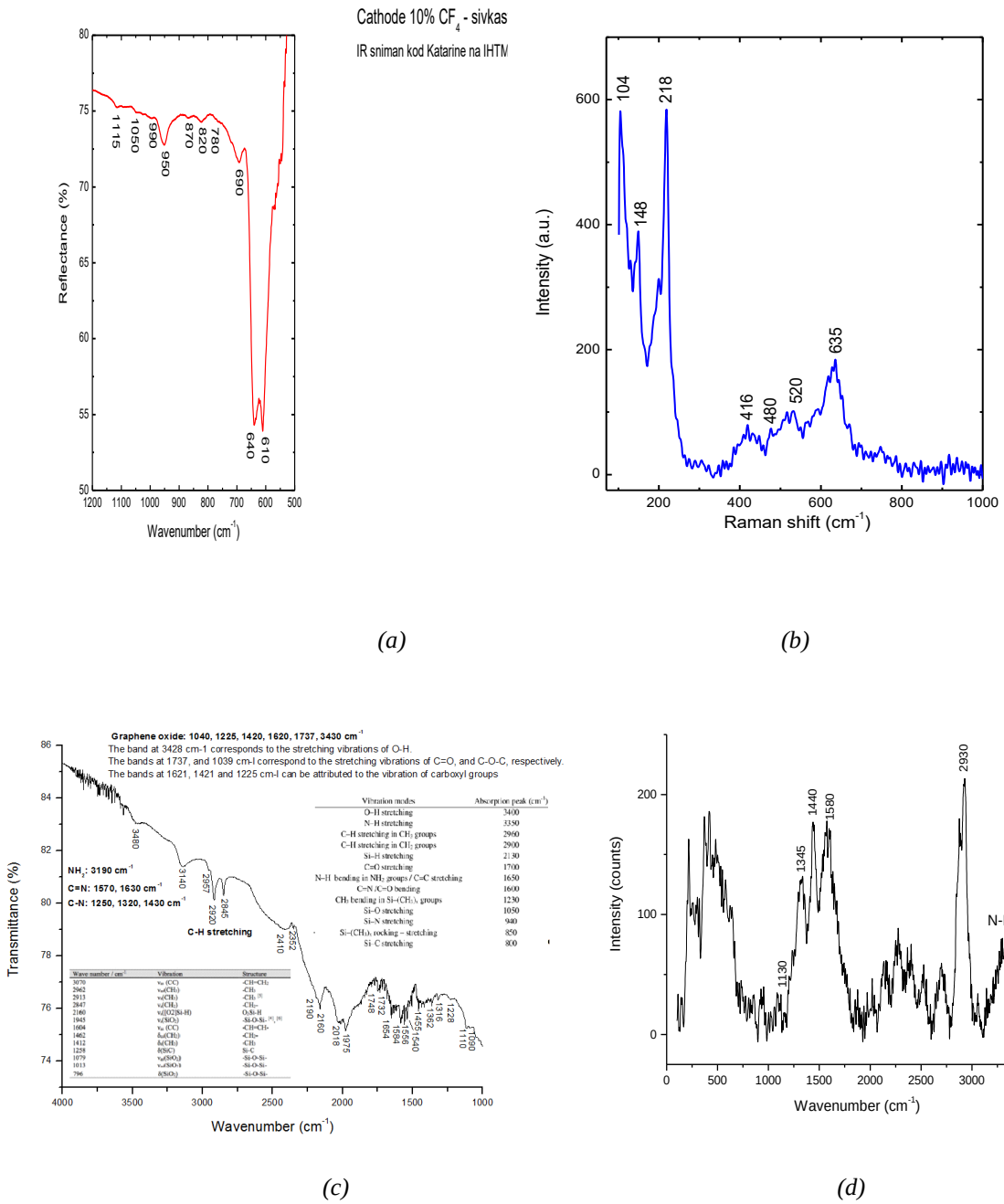

(a) *(b)*

(c) *(d)*

Figure 8. *Vibrational spectra of cathode surface*

(a, c) FTIR in 500-1200 cm^{-1}and 250-3500 cm^{-1} wavenumber interval and (b, d) Raman in 1000-4000 cm^{-1} and 250-3500 cm^{-1} wavenumber interval

Vibrational (FTIR and Raman) spectra of cathode surface are shown in Figure 8 (a - d). The position of vibrational bands is dependent on the force constant of a chemical bond, bond order, types of atoms joined by the bond and reduced mass. In FTIR spectrum copper-oxygen bonds

show characteristic vibrational frequencies in lower wavenumber region 500-1200 cm^{-1}, Fig. 8 (a). Vibrational bands at 640, 820 and 1115 cm^{-1} are attributed to the stretching vibration of Cu-O in Cu_2O molecule. Vibrational bands characteristic for $Cu(OH)_2$ at frequencies at ~ 610, 690 and shoulder at 780 cm^{-1} are due to Cu-O vibrations, while bands around at 3500 cm^{-1} correspond to the vibrations of hydroxyl ions. The band at ~870 cm^{-1} is attributed to bending vibration of Cu–O–H bonds ***(ref.*** *Henrist et al.)*. Bands at 3200, 990, 950 and 670 cm^{-1}, are characteristic for Cu(OH)F molecule. Corresponding vibrational modes characteristic for copper-oxide bonds in Raman spectrum can be detected in wavenumber region 100-650 cm^{-1} Fig. 8 (b). Bands at 104, 148, 218, 416, 520 and 635 cm^{-1} can be assigned to Cu-O-Cu vibrational modes of Cu_2O phase, while bands at ~300 and 480 cm^{-1} originate from $Cu(OH)_2$ phase. *(**Ref**. In Situ Raman Spectroscopy of Copper and Copper Oxide Surfaces during Electrochemical Oxygen Evolution Reaction: Identification of CuIII Oxides as Catalytically Active Species, ACS Catal. 2016, 6, 2473−2481DOI: 10.1021/acscatal.6b00205)*

Information about carbon-based structures can be obtained in wavenumber interval 1000-4000 cm^{-1} Figs. 8 (c, d). Due to numerous vibrational bands in both FTIR and Raman spectra, it can be assumed that various carbon structures from microcrystalline to amorphous (from highly ordered to completely disordered) are formed in plasma chemical reactions and deposited on the cathode surface. As discussed above, XRD results showed low intensity diffraction peak indicating presence of graphene oxide (Fig.7). Graphene oxide ($C_{140}H_{42}O_{20}$) contains various types of oxygenated functional groupsC–OH, C–O–C, C=O and O=C–OH. Bands in FTIR spectrum Fig. 8 (c) that can be assigned to vibrational modes of functional groups in graphene oxide are: 1050, 1315 and 1745 cm^{-1} corresponding to stretching vibrations of C-O-C, C-O and C=O bonds, respectively; 1230, 1360 and 1580 cm^{-1} corresponding to symmetric and asymmetric stretching of COO^- bonds; 1650 cm^{-1} corresponding to stretching vibrations of C=C bonds (or bending modes of watermolecules integrated into graphene oxide structure); 2845, 2920 and shoulder at 2960 cm^{-1} corresponding to symmetric and asymmetric stretching of $C\text{-}H_2$ and $C\text{-}H_3$ bonds; 3480 cm^{-1}corresponding to the stretching vibrations of O-H bonds. Bands at 1975, 2020 and 2190 cm^{-1} can originate from difference in the state of charges between carbon atoms *(**ref.** Biomolecules 2019, 09, 109 ref 26)*. In Raman spectrum Fig. 8 (d) broad band around 500 cm^{-1} indicate presence of amorphous carbon (sp^3 bonded) while bands centered at ~1580 and 1345 cm^{-1} can be assigned to the G-band and D-band, respectively, of graphene oxide. The G-band is linked to the stretching of sp2-hybridised carbon atoms (E2g phonons) while the D-band originates from the disordered graphitic carbon indicating presence of defects.Vibrational modes resulting from their combination and overtone (2D, D+G) are centered in wavenumber interval 2700-2900 cm^{-1}. High intensity band around 2900 cm^{-1} can also be assigned to C-H stretchingvibration, (which can originate from epoxy resin in FR4 laminate). The bands in the interval between D and G peaks are generally attributed to structural defect associated with dislocations, grain boundaries, atomic vacancies and carbon substitution in the structure. Domain boundaries and graphene edges are chemically reactive and can bond different functional groups such as C-OH, $C\text{-}NH_2$ and C-F forming variety of graphene derivatives such as oxidized,

nitrogenated, fluorinated, hydrogenated, etc. Depending of the type and quantity of doped element, derivative graphene structures change their electrical properties such as type of conductivity and the band-gap width. Broad vibrational band centered around 3300 cm^{-1} can be assigned to N-H and O-H vibrations which probably originate from some nitrogen doped graphene/graphene oxide structures as C-N bonds are also detected by ToF-SIMS analysis (Fig. 6). Due to similar frequencies of C–C, C–N and C-F vibrational modes it is hard to detect difference in G-D region between pure and nitrogen or fluorine doped graphene oxide. (*ref. Ferrari*). In FTIR spectrum vibrational bands at ~ 1230, 1320 and 1450 cm^{-1} can be assigned to aromatic C-N stretching modes, bands at ~1560 and 1630 cm^{-1} to C=N stretching modes, while broad band centered around 3140 cm^{-1} corresponds to stretching modes of NH_2 group. As fluorine (F) is detected in significant amount on the cathode surface by elemental analysis techniques (EDX and ToF-SIMS, Figs (4 and 6) it is possible that some fluorinated carbon structures (fluorinated graphene oxide) are formed. Infrared active vibrational modes of C-F can be assigned to bands at: 1100 and 1230 cm^{-1} symmetric and asymmetric stretching of CF_2, respectively, ~1320 C-F stretching, while bands at 1455, 1495, and 1620 cm^{-1} can be associated with aromatic ring with attached fluorine. Due to overlapping of vibrational regions of C-O, C-F and C-N bonds, it is complicated to single out contribution of each mode with certainty. Although Raman spectroscopy is the most valuable technique for characterizing carbon-based structures as it is sensitive to highly symmetric covalent bonds, distinguishing between discussed variety of possible structures requires detail analysis and will be the subject of separate publication. This is of particular interest due to different electrical properties of variously doped graphene derivatives.

Should we put optical micrographs (OM) of cathode surface – dark deposited species with spherical morphology are probably carbon, but we are not sure?

Optical micrographs of cathode surface recorded at different magnifications are shown in Figure 9. Occurrence of dark deposited species showing characteristic spherical morphology (bubble/blister structures) with diameter ranging from 100 to150 microns, can be observed. Further chemical analysis lead to conclusion that the deposits are probably agglomerates of graphite carbon, as presented in Chapter..

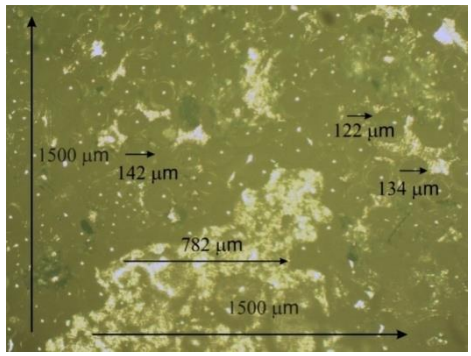

(a)

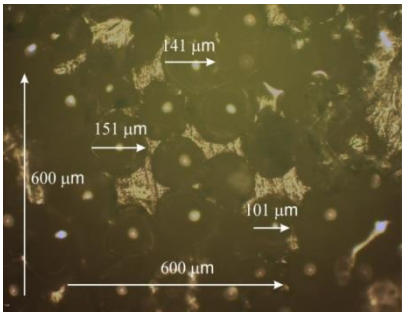

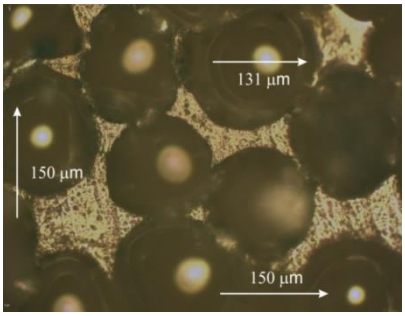

(b) *(c)*

Figure .*Optical micrographs of cathode surface showing presence of deposit.*

Should we compare samples from PNPI (Gennady) with virgin sample from CERN (Katerina)?

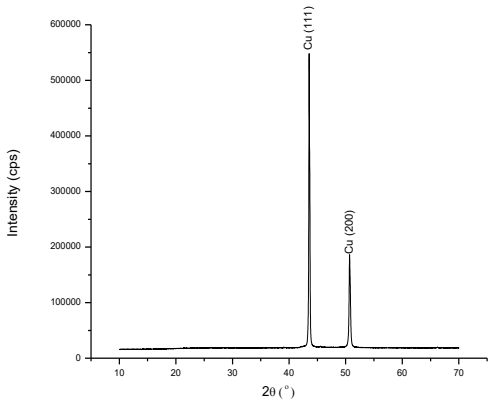

XRD pattern of the virgin cathode (CERN - Katerina's sample)

3.2.Analysis of anode sample

Surface morphology of anode wire sample was analyzed using scanning electron microscopy (SEM), as selected micrographs presented in Figure 10. By inspection of the whole wire, no evidence of significant damage of gold coating and swelling of anode wire due to tungsten oxidation was observed. Imperfections observed in some areas most likely originate from coating process. Secondary electron (SE) image of selected area and corresponding backscattered electron composition (BEC) image with results of elemental analysis (EDS) in characteristic points are given in Figure 10(a, b). SE micrograph shows deposited species ~ 15 µm in length on the wire surface which correspond to dark areas in BEC micrograph. EDS spectra 1, 2 and 3, recorded in discussed dark areas showed high amount of carbon (C ~ 27 - 40 wt%), followed by significant amount of oxygen (O ~ 5 - 11wt%), while silicon was also detected, although in low amount (Si ~ 0.3 wt%). Spectra 4, 5 and 6, recorded in clean area of wire surface showed high concentration of gold (Au ~ 90 wt%) and significantly lower concentration of carbon (C ~ 4 - 9 wt%), while silicon and oxygen were not detected. Detected amount of tungsten is low (W ≤ 1 wt%) apparently originating from minor cracks (~ 0.6-1.6 µm in width) in gold layer in the process of coating Fig. 10(c). Nitrogen is detected in each examined point with relatively constant concentration (N ~4 –6wt%).

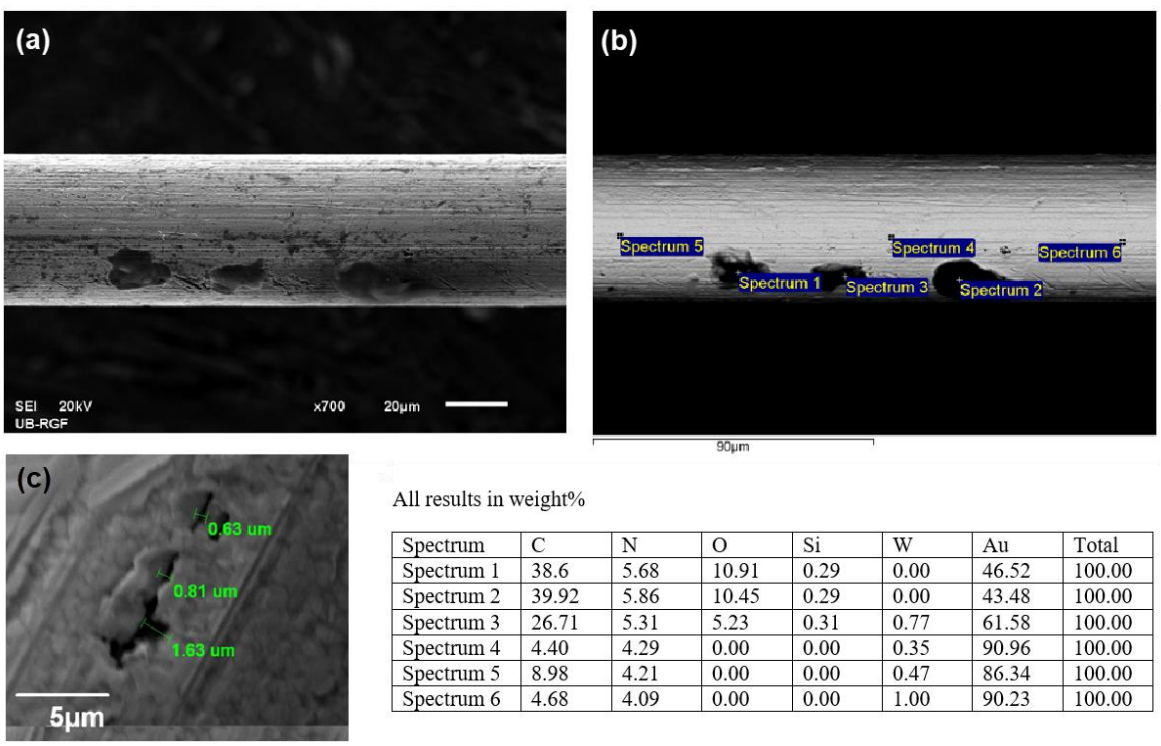

All results in weight%

Spectrum	C	N	O	Si	W	Au	Total
Spectrum 1	38.6	5.68	10.91	0.29	0.00	46.52	100.00
Spectrum 2	39.92	5.86	10.45	0.29	0.00	43.48	100.00
Spectrum 3	26.71	5.31	5.23	0.31	0.77	61.58	100.00
Spectrum 4	4.40	4.29	0.00	0.00	0.35	90.96	100.00
Spectrum 5	8.98	4.21	0.00	0.00	0.47	86.34	100.00
Spectrum 6	4.68	4.09	0.00	0.00	1.00	90.23	100.00

Figure 10. *SEM and EDS analysis of the anode wire surface: (a) secondary electron (SE) image of the selected area on anode surface (magnification x700), (b) corresponding backscattered electron composition (BEC) image with EDS results in characteristic points, (c) micrograph showing minor cracks in gold layer apparently originating from coating process (magnification x3300).*

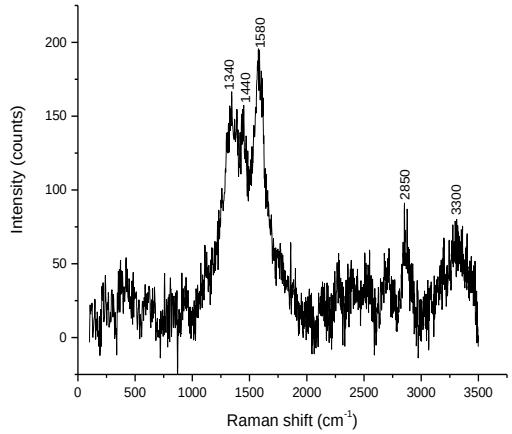

Figure 11. Raman spectrum of the anode wire surface

For carbon deposit characterization Raman spectroscopy was employed. Raman spectra were recorded in several points on the anode wire surface, whereas the summary spectrum is shown in Figure 11. G, D and 2D bands centered around ~1580, 1340 and 2850 cm^{-1}, characteristic for graphene/graphene oxide and bands in interval between them originating from structural defects, are dominant in the spectrum, which is in accordance with EDS and XPS results which showed presence of carbon on the wire surface. Broad band around 3300 cm^{-1}, indicate presence of N-H bonds. Nitrogen was also detected by EDS analysis. As discussed above, vibrational spectroscopic analysis of carbon structures deposited on the surface of both cathode and anode wire samples will be investigated in as separate publication.

Further investigation of the anode surface deposits was done by XPS and (ToF-SIMS).

Figure 12 shows XPS spectra of Au 4f and C 1s from surfaces of a new and an exposed anode. XPS depth profile recorded on the anode is shown in Figure 13. Profiling was done up to about 25 nm depth. The new anode shows the presence of Au, C, O and Si in the top surface layer (Figure Xa). The C, O and Si are probably related with surface contamination.

Au $4f_{7/2}$ spectrum from new anode shows a peak at 84.0 eV probably related with metallic Au matrix, Figure 12a. Carbon C 1s spectrum from a new anode shows presence of peaks at 284.8 eV related with C-C/C-H bonds, a peak at 286 eV (C-O/C-OH bonds), a peak at 287 eV (C=O) and a peak at 289.0 eV (O-C=O/CO3 bonds), Figure 12b. These peaks together present a surface contamination of a new anode. Au $4f_{7/2}$ spectrum from exposed anode shows a peak at 83.6 eV probably related with metallic Au, Figure 12c. Carbon C 1s spectrum has a major peak at 284.8 eV, figure 12d, which is related to C-C/C-H bonds and probably originate from graphite-like deposite on the anode surface, which is evidenced by XPs depth profile bellow.

Figure 13b shows an XPS depth profile up to 23 nm in depth of the exposed anode. Much higher concentration of carbon can be observed on the surface of the exposed anode comparing to a new anode.Relatively high carbon presence on the surface, ~ 80 at%, is probably due to surface contamination. But presence of carbon below from surface to depth of 30 nm, ~ 50 at%, can be attributed to the carbon deposits, similar to the deposits on the cathode, Figure 5. Relatively low concentration of Au, ~ 8 at%, was determined at the anode surface because of the C contamination layer. Removal of surface layers enabled the Au detection and estimated concentration at 20 nm sputtering depth is ~ 50 at%. Oxygen was also identified at the surface, but its concentration significantly decreased below the surface. Tungsten was not identified at the sampling area by the XPS method, which implies there was no breach in the outer Au layer.

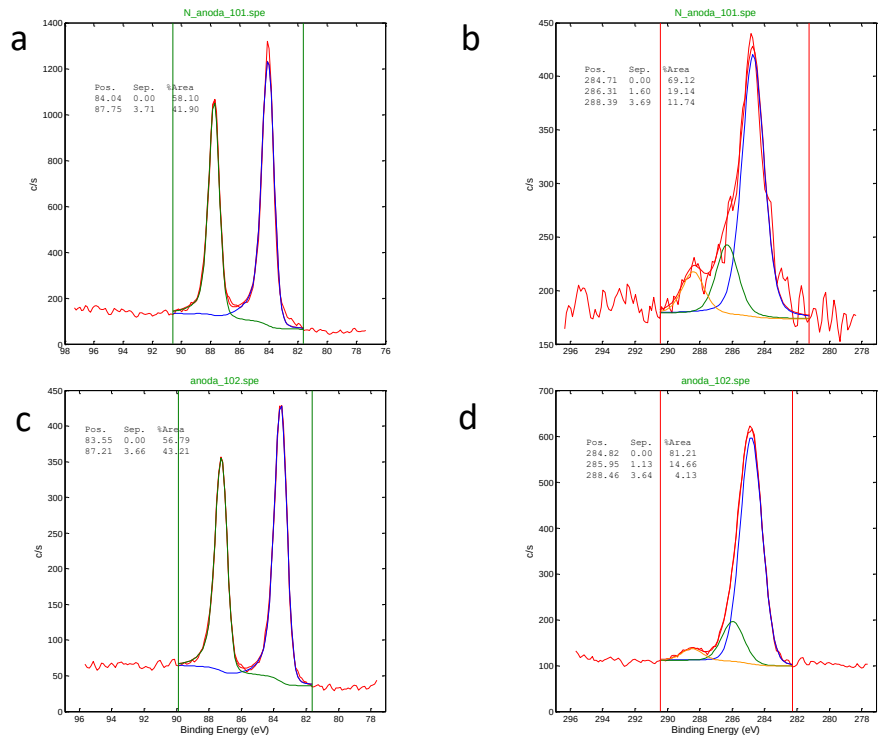

Figure 12. XPS spectra Au 4f and C 1s from the surface of (a, b) new and (c, d) exposed anode.

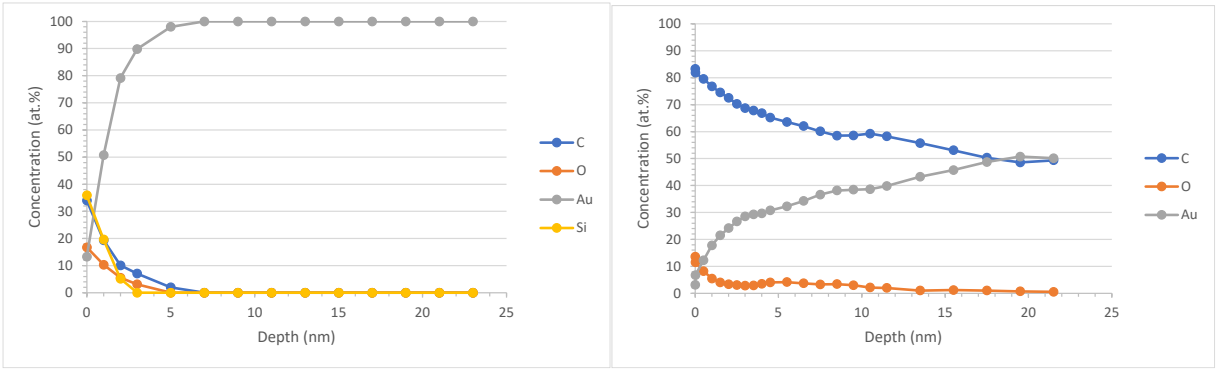

Figure 13. XPS depth profile recorded on the unexposed anode and anode subjected to a long term exposure of β-source ^{90}Sr in the gas mixture of 40% Ar, 50% CO_2 and 10%CF_4, in the course of CSC longevity tests.

SIMS spectra of positive and negative ions from the anode surface are presented in Figure 14. The conclusion is that the anode surface is contaminated by PDMS compound, which probably originates from ...

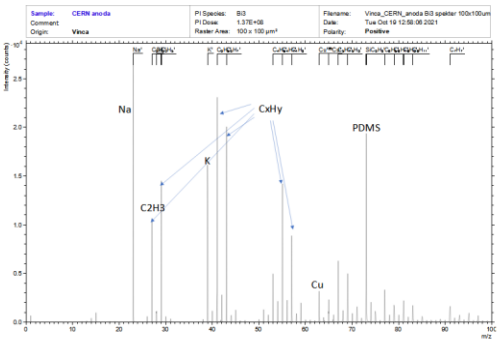

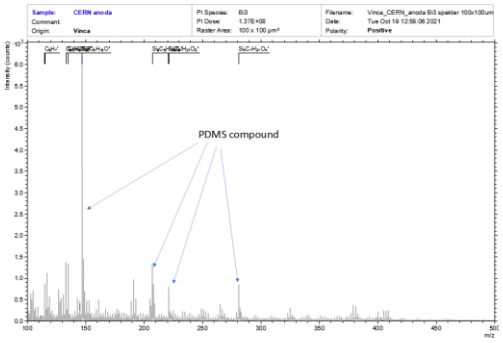

a)

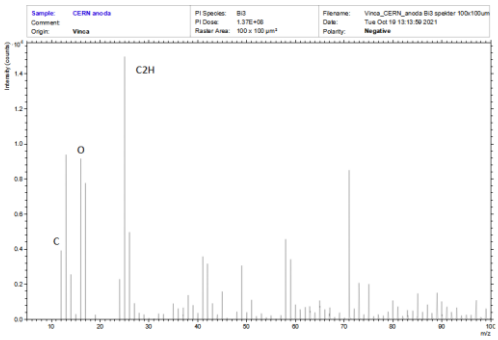

b)

c)

Figure 13. SIMS spectra of (a,b) positive and (c) negative ions from the surface of anode subjected to a long term exposure of β-source ^{90}Sr in the gas mixture of 40% Ar, 50% CO_2 and 10%CF_4, in the course of CSC longevity tests.